

Glassy dynamics near the learnability transition in deep recurrent networks

John Hertz*

*Nordita, Stockholm University and KTH, Sweden
Niels Bohr Institute, University of Copenhagen, Denmark*

Joanna Tyrcha†

Matematiska institutionen, Stockholm University, Sweden

(Dated: December 16, 2024)

Abstract

We examine learning dynamics in deep recurrent networks, focusing on the behavior near the learnability transition. The training data are Bach chorales in 4-part harmony, and the learning is by stochastic gradient descent. The negative log-likelihood exhibits power-law decay at long learning times, with a power that depends on depth (the number of layers) d and width (the number of hidden units per of layer) w . When the network is underparametrized (too small to learn the data), the power law approach is to a positive asymptotic value. We find that, for a given depth, the learning time appears to diverge proportional to $1/(w - w_c)$ as w approaches a critical value w_c from above. w_c is a decreasing function of the number of layers and the number of hidden units per layer. We also study aging dynamics (the slowing-down of fluctuations as the time since the beginning of learning grows). We consider a system that has been learning for a time τ_w and measure the fluctuations of the weight values in a time interval of length τ after τ_w . In the underparametrized phase, we find that they are well-described by a single function of τ/τ_w , independent of τ_w , consistent with the weak ergodicity breaking seen frequently in glassy systems. This scaling persists for short times in the overparametrized phase but breaks down at long times.

I. INTRODUCTION

Recurrent neural networks are an attractive tool for modeling dynamical systems based on time-series data. They contain implicitly a mechanism for storing and using information about past states of the system to generate the next state. This property is essential, for example, in applications to music generation, where information about the distant past can be necessary to generate the correct temporal structure in the near future.

In understanding any learning network, an essential feature is the learnability transition: the boundary in hyperparameter space separating regions where a training set can be learned from regions where it can't be. Some work [1–3] has explored aspects of this problem for standard

layered networks. In our work here, we study it in a class of layered networks with recurrent interactions within the layers.

In our work we have trained recurrent nets to imitate Bach's chorales: sequences of chords in 4-part harmony. This has led us to study the phase diagram of these networks in the space defined by their width and depth. In particular, we investigate the learnability transition between underparametrized and overparametrized networks with d feedforward connection layers and w recurrently connected hidden units in each layer. We call d the depth and w the width of the network. We study networks with depths 1, 2, 5, and 10, and for each depth value we vary the width around the critical value w_c required to achieve correct learning. We find critical slowing down near the transition and aging in the underparametrized phaselike that in a class of mean-field spin-glass models [4–6].

The paper is organized as follows. In Sec. II

* hertz@nbi.ku.dk

† joanna@math.su.se

we describe the model networks we study, the training data, and how they are trained. In Sec. III we present general features of the training results: the shapes of the learning curves for under-, over- and critically parametrized networks, showing how they depend on network depth. Sec. IV then explains how we observe critical slowing-down and estimate the critical layer size w_c for depths 1, 2 and 5. Sec. V is about aging. We consider a network that has been learning for a time τ_w (its “age”) and then measure, at longer times, the fluctuations in the connection weight values around their values at τ_w . Finally, Sec. VI is devoted to discussion of the results, particularly with respect to theoretical findings for spin-glass models, and general conclusions.

II. MODELS AND TRAINING

Our networks have feed-forward connections between layers and fully recurrent connections within each layer. In this architecture, the recurrence within layers allows the hidden units to store information about past time steps and thereby better predict the next step. The multilayer structure then permits this advantage to be exploited in different ways in different layers, giving the model the potential to describe more complex long-time dynamics than a single-layer recurrent model could.

Letting the hidden layer index i run from 0 to $d - 1$, we denote the feedforward connection matrix to each layer i by J_i and the recurrent connection matrix within each layer by M_i . (We do not find it necessary to use biases except for the final output.) We have studied networks of depth 1, 2, 5, and 10 with widths ranging from 25 to 200. The hyperbolic tangent is taken as the activation function for all units.

For the learning data, we use the Bach Chorale data set studied by Boulanger-Lewandowski *et al* [7], as described in Appendix A. The raw 54-dimensional input input vectors $S_0(t)$ in the training set represent the chords in the chorales, and each example is a transition from one chord to the succeeding one. In running the network the $S_0(t)$ are rescaled

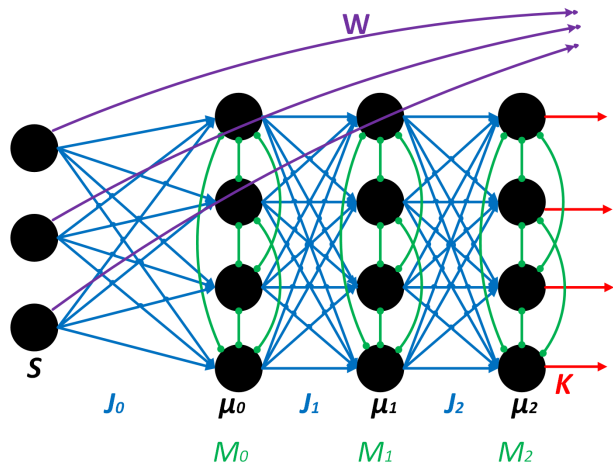


Figure 1. Schematic graph of our network architecture. The blue lines represent feedforward connections, and each green line represents a pair of (generally unequal) intralayer interactions $J_{l,ab}$ and $J_{l,ba}$. The purple (W) and red (K) connections feed into the output units as described by Eq. 3.

to give input vectors $S(t)$ of zero mean and unit variance. Thus, the first layer-to-layer connection matrix, J_0 , is $w \times 54$. The rest of the J matrices are $w \times w$, as are the intralayer recurrent interaction matrices M . There is also a 54-dimensional output bias vector denoted h_0 and a $54 \times w$ matrix, denoted by K , connecting the final layer with the output units, and a 54×54 matrix W connecting directly from the inputs S to the outputs. The network is pictured schematically in Fig. 1.

Then, with μ_l denoting the activation vector of layer l and O the output, the dynamics of the network are given by

$$\mu_0(t) = \tanh[J_0 S(t) + M_0 \mu_0(t-1)] \quad (1)$$

$$\mu_l(t) = \tanh[J_l \mu_{l-1}(t) + M_l \mu_l(t-1)] \quad (2)$$

for $l < d$, and

$$O(t) = \tanh[K \mu_{d-1}(t) + W S(t) + h_0] \quad (3)$$

(with the common convention that the \tanh acts unit by unit).

We trained our networks using back propagation through time (BPTT) and stochastic gradient descent (SGD) with a minibatch size of 300

chord transitions and a negative log likelihood loss function. In training, the next chord in the chorale, $S_0(t + 1)$, is used as the output target at step t . When the trained network is used to generate new music, the output at one time step is fed back as the input at the next step.

In order to avoid exploding or vanishing gradients in the learning, we initialized all our matrices J_i (except $i = 0$) and M_i as orthogonal, as was done for linear non-recurrent feedforward networks by Saxe *et al* [8] and extended to layered networks with general activation functions by Pennington *et al* [9]. Here, we found that stability required us to enforce continued orthogonality of the M_i (though not the J_i) under learning.

The training process is described in greater detail in Appendix B.

III. GENERAL FEATURES OF THE LEARNING

We have performed learning on networks of depth $d = 1, 2$, and 5 , training until the negative log likelihood (NLL) fell to a value 0.01 or less. (Here and henceforth whenever we write “NLL” we will mean its value in bits per output unit per time step.) The 0.01 -bit value corresponded to an accuracy of approximately 99.9% . This choice was dictated by the fact that we found that an NLL of around this size was necessary for the network to generate plausible-sounding music when run in closed-loop mode.

Panels (a), (b), and (c) of Fig. 2 shows typical learning curves for the networks of three depths. In each graph, we show cases where the network is underparametrized, overparametrized, and somewhere in between, generally not far from the critical value for that depth. The learning time variable τ is in units of the inverse learning rate, i.e.,

$$\tau(n) = \sum_{m < n} \frac{1}{\eta(m)}, \quad (4)$$

where n and m count the number of iterations and $\eta(m)$ is the learning rate at step m . We will refer to τ as *proper time*.

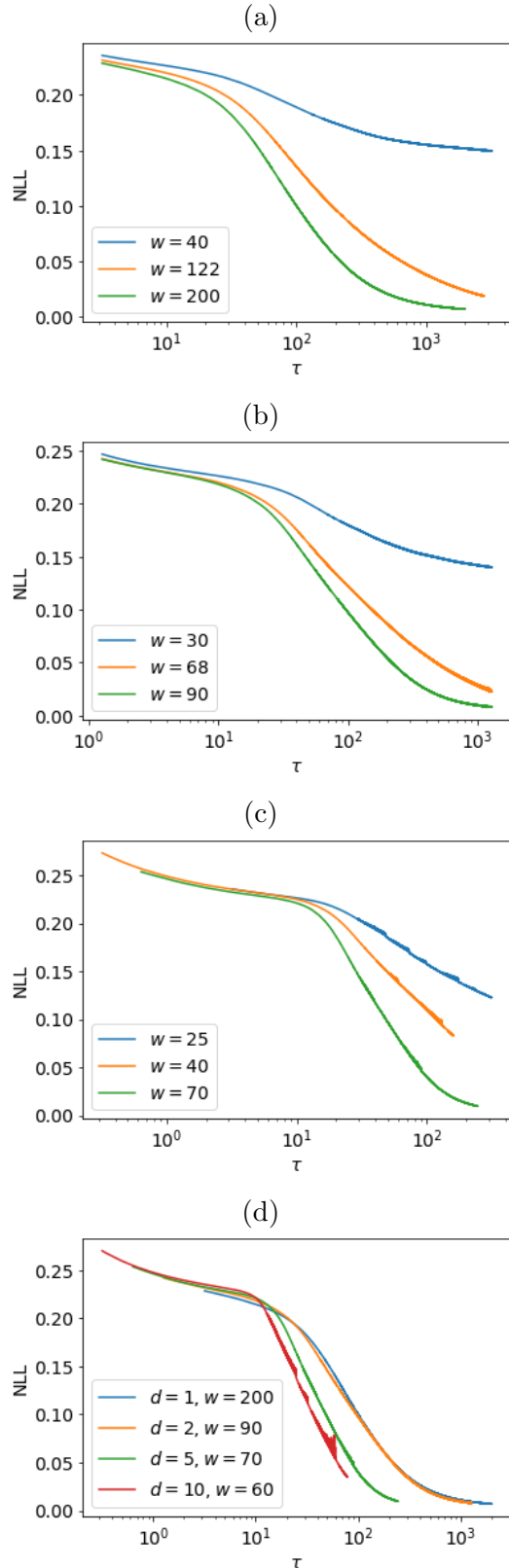


Figure 2. Sample learning curves for (a) $d = 1$, (b) $d = 2$, and (c) $d = 5$. (d): Learning curves for overparametrized cases for depths $d = 1, 2, 5$, and 10 . The scale for the learning time τ is logarithmic.

Increasing the network depth shrinks the learning time as measured by the variable τ . Panel (d) of Fig. 2 shows this effect (though there is apparently no significant difference between $d = 1$ and $d = 2$).

We found it that it was necessary to reduce the learning rate η strongly during learning in order to maintain smooth learning curves, and that this constraint grows more severe with increasing depth. (The curve in Fig. 2 for $d = 10$ illustrates the kind of noise that can occur if the learning rate is not reduced strongly enough.) This effect, coupled with the fact that deeper networks require more calculations to begin with, means that the actual computation time grows rather than shrinking with increasing depth.

For underparametrized cases, we see that, as expected, the NLL remains far from zero even for the longest learning times. For $d = 2$ and $w = 30$ we were able, using the very long learning time calculations done for the aging calculations to be described in Sect. 5, to fit the loss as a power-law decay to a value $NLL_\infty = 0.1265$ with an exponent 0.52.

In the neighborhood of the critical layer size, it is evident that the learning becomes very slow, and direct measurement of the asymptotic form of the learning curve becomes computationally inaccessible. We are forced to rely on extrapolations from the overparametrized side to estimate the critical width, as we describe in the next section. However, again in the $d = 2$ case we have access to very long-time learning data for the very-nearly critical width value $w_c = 68$ and obtain a power law fit to a very small asymptotic value $NLL_\infty = 0.002$ with an exponent 0.83.

For the overparametrized cases, power-law decay of the NLL is seen for all three values of w when it is in the range 0.02 to 0.1. For $d = 1$ and $w = 200$, we found an exponent 1.04 ± 0.01 , and for $d = 5$ and $w = 70$ we found an exponent 1.57 ± 0.02 . For $d = 2$ and $w = 90$, we were again able to obtain more complete data from the aging calculations. They show power-law decay to a limit $NLL_\infty = 0.0035$ with an exponent 1.16.

The measured long-learning-time NLLs and the respective power-law fits for the three values of w for $d = 2$ are shown in Fig. 3. The overall

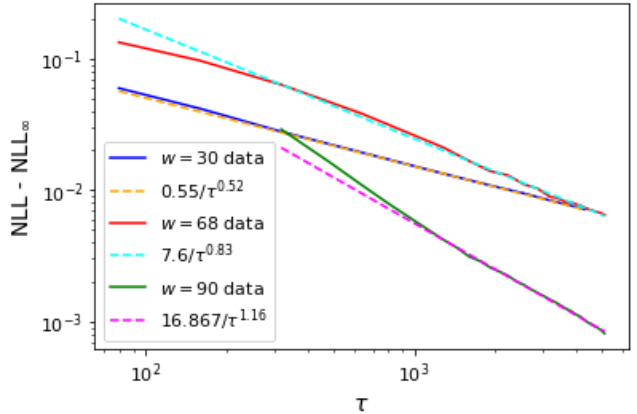


Figure 3. Asymptotic power-law approach of the NLL to asymptotic values N_∞ for $d = 2$, $w = 30$, 68, and 90. NLL values were measured every 4×10^5 learning steps. At the longest times ($\tau > 2 \times 10^3$) the measurements were averaged over 1000 steps to reduce the effect of SGD noise. The dashed orange lines are the power-law fits.

pattern of these results suggests that the asymptotic decay is always power-law and that the exponent increases with both d and w . However, the detailed dependence on d and w remains to be explored.

Because of the stochasticity of SGD learning, our learning curves are always intrinsically noisy. The noise is not visible at the resolution of the plots in Fig. 2, but at the very small NLLs achieved at very long times, a closer look at the data reveals fluctuations that are not negligible compared to the time-averaged mean values. Fig. 4 shows a 1000-step graph of the measured loss after 3.2×10^6 learning steps for $d = 2$ and $w = 90$, for minibatch sizes $p = 75$ and 300. As expected, smaller batches lead to greater noise and larger mean error. We chose a larger-than-usual batch size of 300 in our calculations (except this one) to reduce this effect. Nevertheless, we still had to use 1000-step mean values of the measured NLLs at the longest times to get the smooth results seen in Fig. 3.

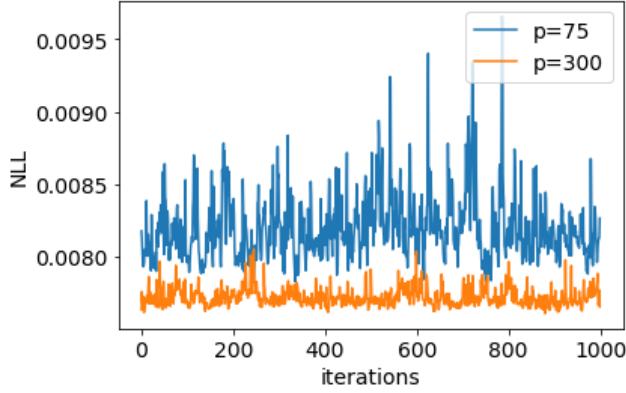


Figure 4. Fluctuating NLL for SGD minibatch sizes 75 and 300.

IV. CRITICAL DYNAMICS

In order to make estimates of the critical values w_c of the number w of hidden units per layer for given depth d , we studied systems with $d = 1, 2$ and 5 . For each d we trained the networks for a range of values of w . We recorded the proper times required for the NLL to reach 0.01, 0.02, 0.03, 0.05 and 0.1. All these times grew dramatically as w was reduced. Plotting the reciprocals of these learning times as functions of w , revealed that they all varied nearly linearly with w . These measurements are shown as the black dots in Fig. 5.

We made quadratic regression fits to each set of learning-time measurements. These are shown as the colored curves in Fig. 5. The place where the curve for some NLL value crosses the w axis is our estimate of the smallest w for which the NLL can reach that value. The graphs show that the system exhibits critical slowing down as one approaches the critical value of w . Such critical dynamics also occur in many spin-glass models, for example, near the Almeida-Thouless (AT) line [10] in the temperature-field plane of the Sherrington-Kirkpatrick spin glass [11]. The same kind of transition also occurs in simple perceptrons near their capacity limit [12, 13]. Other systems with critical slowing down near AT lines in their phase diagrams include spherical p-spin glasses in an external field [5] or in the presence of a ferromagnetic interaction [6] and a particle moving in a correlated random potential in

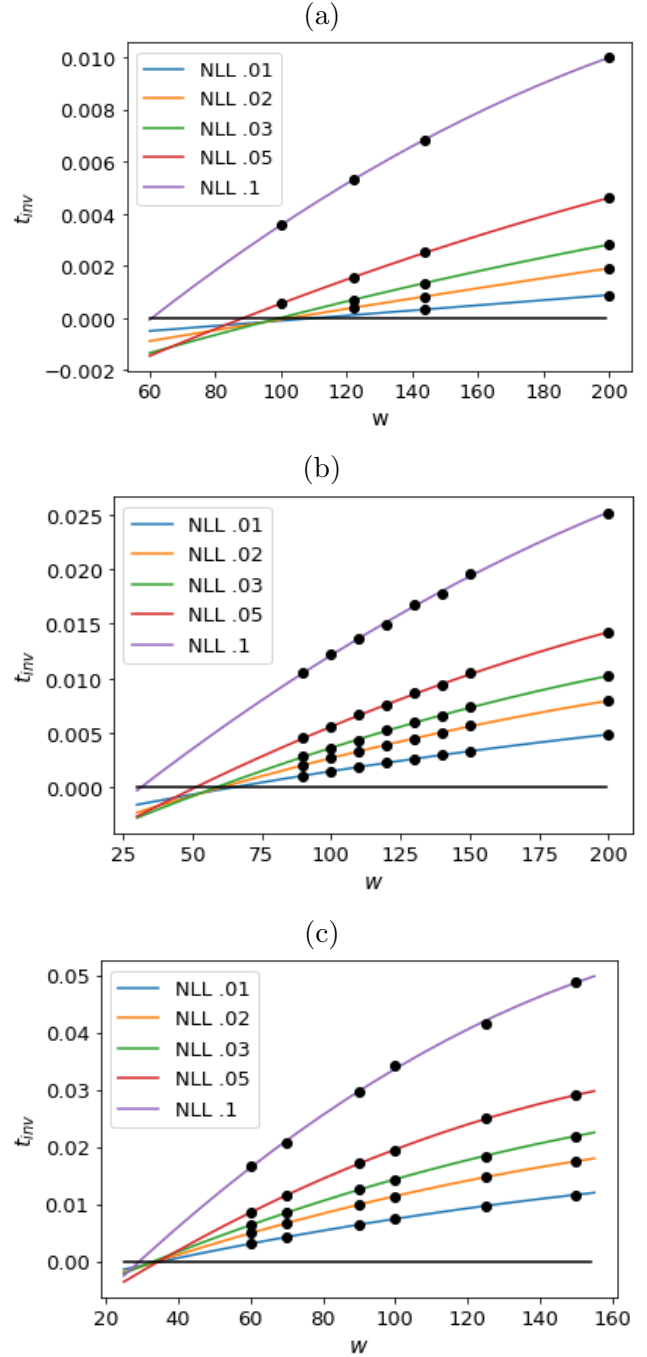


Figure 5. Inverse learning times τ_{inv} required to reach to reach NLL values 0.01, 0.02, 0.03, 0.05 and 0.1, as functions of w for (a) $d = 1$, (b) $d = 2$, and (c) $d = 5$. Black dots mark the results of the learning runs, and the colored curves are quadratic regression fits to them. The points where these curves cross the w axis are our estimates of w_c .

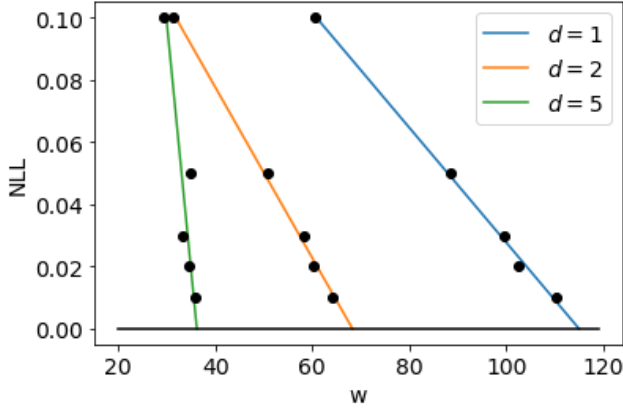


Figure 6. NLL vs width for $d = 1, 2$ and 5 .

a high-dimensional space [4]. We will return to this point in the Discussion section.

It is evident, for all the terminal NLL values we have considered, that the deeper the network, the smaller the critical w required to learn the data. This much is not surprising, as deeper networks have more parameters. But there is more to the story. If we compare the number of parameters in the three NLL=0.01 critical networks, we find that the single-hidden layer one ($w_c = 110.21$) has 20890, the two-hidden-layer one ($w_c = 64.192$) has 18080, and the 5-hidden-layer one ($w_c = 35.735$) has 15040 parameters. (Here, in counting parameters, we assign the M matrices a number $w(w-1)/2$, where the division by 2 is because they are constrained to be orthogonal.) Thus, depth is apparently more effective than width, at least for these data and this class of networks.

For each depth, we performed linear regression of the estimated critical values w_c against the respective NLL values. Fig. 6 shows the results, plotting w_c on the x axis and the NLL values on the y axis. These lines are estimates of the way the error (NLL) varies as one approaches the critical points from the underparametrized side. At least for $d = 1$ and 2 , the linear dependence assumed in the regression appears to be reasonable, though for $d = 5$ we cannot draw any immediate conclusion. We have to be cautious here because the data points in this graph are themselves results of regression and extrapolation on the data, but it at least appears clear that the deeper the network, the sharper the transition

is.

V. AGING

A pervasive feature of glassy systems is aging, i.e. the slowing down of fluctuations over long timescales [14]. Baity-Jesi *et al* [3] explored this phenomenon in some standard layered feed-forward networks. Their networks did not have recurrent dynamics, and they were all either strongly overparameterized or (in a single case) strongly underparametrized. Here we study the transition region for our networks, using the same approach that they took. The procedure was as follows: We made long learning runs of up to 3.2×10^6 iterations, saving the network weight values after 2×10^5 , 4×10^5 , 8×10^5 , 1.6×10^6 and 3.2×10^6 iterations. These run durations, converted to proper time τ , are conventionally called “waiting times”, and we denote them by τ_w . Then, taking each of these saved networks as an initial condition, we measured the growth of the mean-square weight fluctuations

$$D(\tau_w, \tau_w + \tau) = \langle [w_{ij}(\tau_w + \tau) - w_{ij}(\tau_w)]^2 \rangle_{ij}, \quad (5)$$

as the learning was run for an additional time τ . The maximum τ was always at least three times the length τ_w of the initial run (and greater than that for the smaller values of τ_w).

To quantify how the growth of the subsequent fluctuations with τ depends on the waiting time τ_w we measured the increase in the weight change variance at each increase of τ relative to the intrinsic weight fluctuations inherent in SGD at that time. At time τ , these fluctuations have a variance (a kind of temperature)

$$\Gamma(\tau) = \frac{1}{p} \left\langle \text{var}_\mu \left(\frac{\partial E_\mu(\tau)}{\partial w_{ij}} \right) \right\rangle_{ij}. \quad (6)$$

Here E_μ is the cost function evaluated on training example μ , w_{ij} denotes a weight in the network, p is the minibatch size, and the variance is over the batch of training examples for each weight. Thus, we should evaluate the quantity

$$\Delta(\tau_w, \tau_w + \tau) = \int_{\tau_w}^{\tau_w + \tau} d\tau' \frac{\partial D(\tau_w, \tau_w + \tau') / \partial \tau'}{\Gamma(\tau')} \quad (7)$$

(where the integral notation really means a sum over individual learning steps). Calculating Δ this way, rather than just taking $\Delta \propto D$, can be thought of as removing the effect of the varying noise level Γ produced by SGD, permitting comparison with ordinary models with constant noise (constant temperature).

In practice, it was computationally too costly to evaluate $\Gamma(\tau')$ at every iteration. However, we found that Γ varies rather slowly with τ , so we only evaluated it every 10000 steps. Baity-Jesi *et al* employed the approximation $\Gamma(\tau) = \Gamma(\tau_w)$, which we find to be reasonable at very large τ for overparametrized models but not for all the cases we studied.

We have performed calculations for networks with two hidden layers, with widths 30, 68 and 90, to illustrate the phenomenon for moderately underparameterized, nearly critical, and moderately overparametrized cases, respectively. Following the example of Baity-Jesi *et al* [3], we show the results as log-log plots in the first two columns of Fig. 7. We also show the corresponding linear plots of $\Delta(\tau/\tau_w)$ in the third column.

Two universal features of these plots are immediately evident. The first (which can be seen in all the graphs in the left-hand column), is that the plots for different values of τ_w collapse onto a common function of τ for $\tau \ll \tau_w$. The data at very short times are rather noisy, but we estimate that $\Delta \propto \tau^\alpha$ with $\alpha \approx 0.7$, with an uncertainty of around ± 0.1 for all three values of w . We do not see any evidence that α depends on w .

The second noteworthy feature is the tendency to a collapse onto a single function of τ/τ_w at longer times. This is seen most clearly for the underdetermined case $w = 30$ (panels (b) and (c)). This behavior is consistent with the aging behavior found in a wide class of spin glass models [14].

For the near-critical $w = 68$ the behavior is similar. It is difficult to see any breakdown of the collapse onto a single function of τ/τ_w in the loglog plot (e), but one can see in the linear plot (f) that the collapse is not as clean as for $w = 30$.

For the overparametrized case $w = 90$, one can see that the collapse breaks down more

strongly. It appears to hold for the shortest values of τ_w but fails dramatically, as is visible in the red and violet curves in panel (i). Such a transition was also observed for strongly overparametrized models in the findings of Baity-Jesi *et al*.

To summarize: In the underdetermined phase ($w = 30$), we find aging behavior something like that in p-spin spherical models, with a collapse onto a single function of τ/τ_w for τ of order τ_w or greater. By analogy with these problems, we might expect aging to disappear at and above the critical $w \approx 68$. However, even well into the overdetermined phase ($w = 90$), aging holds at least approximately at the shorter values of τ_w for which we have measured Δ , though it breaks down as expected for the largest τ_w .

We have also measured the SGD noise $\Gamma(\tau)$ in our aging runs. Fig. 8 shows how it varies under learning for $w = 30, 68$ and 90 . We note a general tendency for Γ to grow with τ , but with a decreasing rate of growth and (at least for $w = 30$ and 90) an eventual levelling off. For the overparametrized case $w = 90$, it even appears to fall a bit at the longest measured times. It is also interesting that the critical case $w = 68$ is the noisiest, and the noise variance value varies quite noisily itself.

VI. DISCUSSION

Our main results here are (1) the critical slowing-down that we see upon approaching the transition from the overparameterized side and (2) the finding of aging, specifically the dependence of the normalized growth of fluctuations Δ on the ratio τ/τ_w . The first of these suggests that the transition is like that in a spin glass at an Almeida-Thouless (AT) line [10]. In a replica-based equilibrium theory, spin-glass order parameter fluctuations diverge as one approaches such a line, and this is reflected in the dynamics as critical slowing-down, as first shown for the Sherrington-Kirkpatrick model [11] by Sompolinsky and Zippelius [15]. The second suggests that the underparametrized phase would have, in a replica-based description, 1-step replica symmetry breaking (RSB).

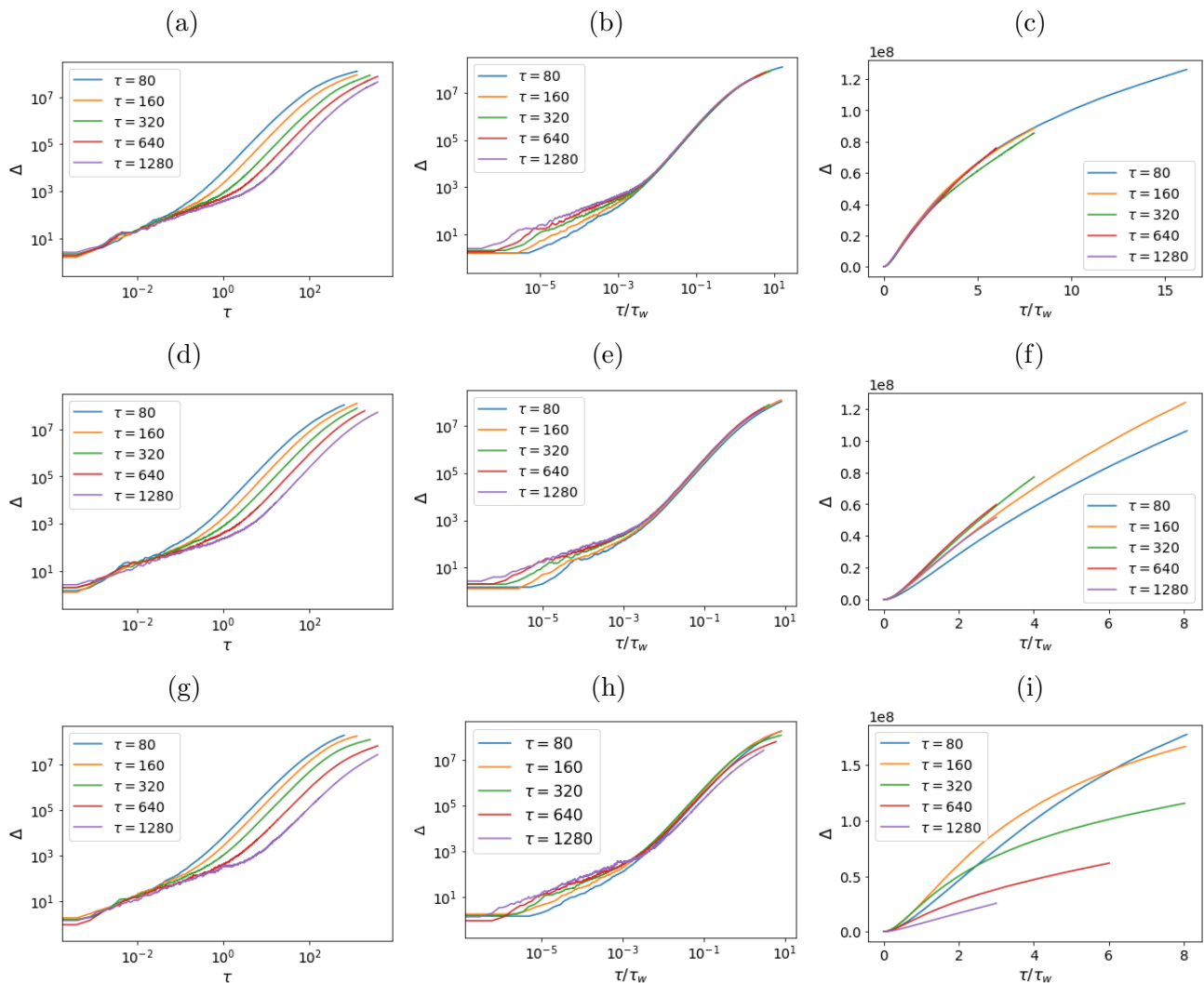


Figure 7. Aging for $d = 2$, $\tau_w = 80, 160, 320, 640$, and 1280 . (a) $w = 30$, loglog plot of Δ as function of τ , (b): as in (a) but Δ plotted as function of τ/τ_w , (c): like (b) but linear plot; (d), (e) and (f): like (a), (b) and (c) but for $w = 68$; (g), (h) and (i): like (a), (b), and (c) but for $w = 90$.

Quite generally, the dynamics of such a state exhibit what is called “weak ergodicity breaking” of which aging is a consequence [14].

We know of two classes of models that have AT lines in their phase diagrams separating an ergodic phase from one with weak ergodicity breaking and 1-step RSB. One is p-spin glasses in the presence of either an external field [5] or an internal mean field caused by a ferromagnetic interaction [6], and the other a particle diffusing in the presence of a short-range-correlated random potential in an N -dimensional space in the limit $N \rightarrow \infty$ [4]. The two kinds of models are closely related mathematically.

It is necessary here to mention a technical point: The p-spin glass models here have continuous-valued spins, and there is a chemical potential μ which is adjusted so as to enforce the spherical constraint $\sum_i s_i^2 = N$. The chemical potential is also present in the model of the particle moving in the random potential. It then keeps the magnitude of the displacement of the particle finite, but it is not adjusted to constrain it to a particular value. One can also consider the unconstrained version of that model, i.e., $\mu = 0$. This has not been done in any p-spin glass model, but Cugliandolo and Le Doussal did so for the particle moving in the correlated

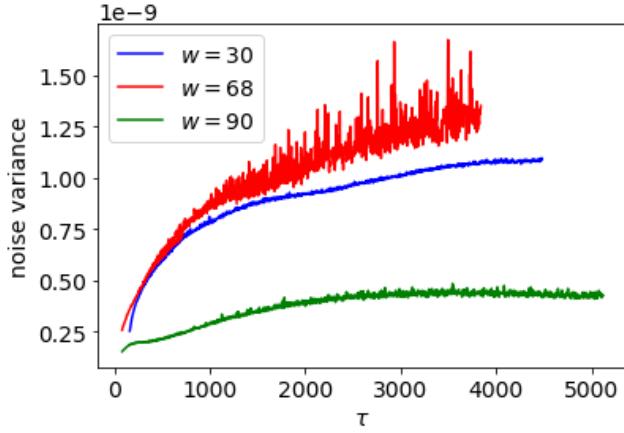


Figure 8. Variation of the SGD noise variance with time.

random potential. In our network, while the M matrices have fixed mean square values because of the orthogonality constraint that we enforce, the J matrices are not constrained. Thus, our model is more like the unconstrained case in their model.

For both classes of models it has been found that $\Delta(\tau/\tau_w)$ exhibits singular power-law growth in the aging regime growth for small τ/τ_w [4, 6]. Although a full investigation of the large τ/τ_w regime is beyond the reach of our computational resources, we have been able to measure Δ for times up to $16\tau_w$ for $\tau_w = 80$ in the underdetermined case $w = 30$. The predicted singular growth of Δ at very small τ/τ_w is not immediately evident in the data, since the transition from the short-time to the aging regime is not sharp for such a small τ_w ; However, at values of τ/τ_w approximately in the range 1 to 6, a good fit to a power law with exponent 0.66 is possible if we take the beginning of the aging regime to be at $\tau = 0.6\tau_w$, as shown in Fig. 8.

Cugliandolo and Le Doussal found that in their unconstrained model Δ grows like $\log(\tau/\tau_w)$ in the limit $\tau \gg \tau_w$. We find that it is possible to fit the data with a $\log(\tau/\tau_w)$ dependence for $\tau/\tau_w > 10$, as also shown in Fig. 9. Of course, one would need data over a much longer time range to prove the logarithmic form generally, and we cannot exclude the possibility that Δ saturates at some finite value (as in spheri-

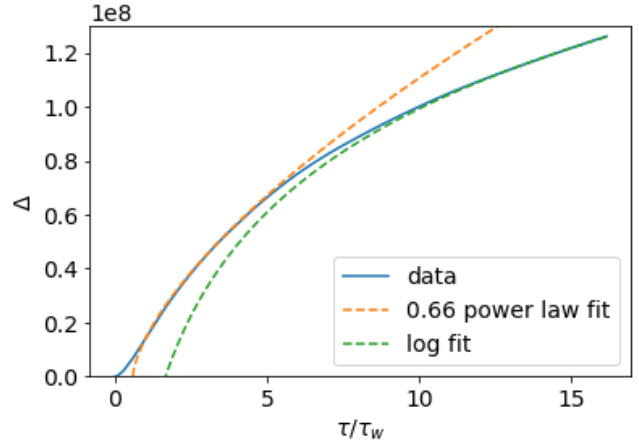


Figure 9. Fits to $\Delta(\tau/\tau_w)$ for small (1-6) and large (10-16) values of τ/τ_w .

cal models). However, at least we can see that the available data are not inconsistent with the logarithmic theoretical prediction.

Baity-Jesi *et al* [3] compared the learning dynamics they observed in layered networks without recurrence with those of the p-spin glass without a field (external or internal). They rejected the hypothesis that the two systems had the same kind of behaviour, on the grounds that the aging they had found in their highly overparametrized models stopped at very long times $t > t_2$, when the tasks were finally learned. Our results at the longest times in our overparameterized model also show such a breakdown, though we would need much longer runs to verify the similarity in detail. They also studied one strongly underparametrized network and found spin-glass-like aging consistent with what we have observed here for the 2-layer 30-hidden unit per layer network. Thus, while they did not study networks near the learnability threshold, our findings and theirs are fully compatible. In particular, we do not find any evidence that that the learning dynamics depend on whether the network has recurrent dynamics or not. In either case, it seems that the essential features of the nonlinear learning dynamics may be captured by the problem of a particle moving in a short-range-correlated random potential in high dimensionality.

We should also note a problem we have en-

countered and not yet dealt with satisfactorily. We have found it necessary to use very small learning rates (at least an order of magnitude smaller than for networks without recurrent dynamics) to get smooth learning. This effect gets stronger with increasing network depth and has prevented us from any systematic study of networks with more than 5 layers. It is also exacerbated near the transition, slowing the computation down even more than the critical slowing down alone would imply.

Finally, we would like to remark that the exploration of phase diagrams in hyperparameter space and the transitions between phases in them more generally could help in understanding in which regions networks perform stable computations free of undesirable fluctuations and biases, and in which ones they do not, thereby improving the usefulness and reliability of AI systems.

Appendix A: Data

The data were downloaded from the Bengio lab in Montreal, following the link [16] in their 2012 ICML paper [7]. In this work, we used the first 80 chorales of their collection. In their data, the music was quantized for simplicity into quarter notes, so half notes and full notes were represented by 2 or 4 repeated quarter notes. Despite this brutal simplification, one can still recognize Bach’s when listening to the music in this form.

In a preliminary calculation, the chorales were converted into sequences of 54-dimensional binary-valued vectors. Each direction in this space corresponded to a key on a piano keyboard (54-dimensional rather than 88-dimensional because modern pianos didn’t yet exist in Bach’s time and he only used 54 notes in these compositions). For each component, a value $S_i = +1$ indicated that the corresponding key should be played, and a value $S_i = -1$ indicated that it shouldn’t be. Most of the music consisted of 4-note chords (for 4-part chorale singing), so in most of the data vectors, 4 of the components S_i were equal to +1, but there were some chords in which some of the voices were silent, so fewer of

the components were +1. For each chorale, the training input vectors consisted of all the chords $S_i(t)$ in the sequence they were played in except the last one, and the target output for each input was the chord $S_i(t+1)$ at the following step. The full 80-chorale training set consisted of 4597 such input-target pairs.

Appendix B: Learning algorithm

We took the negative log likelihood (NLL) of the training data sequence under the model as the cost function for the learning. The weight change rules for stochastic gradient (SGD) learning can then be obtained by straightforward differentiation. For W , K and h_0 they involve the output field

$$H_i(t) = \sum_a K_{ia} \mu_{d-1}(t) + \sum_j W_{ij} S_j(t) + h_{0,i} \tag{B1}$$

directly in the target error $\epsilon_i(t) = [S_i(t+1) - \tanh H_i(t)]$:

$$\Delta W_{ij} = \frac{\eta}{p} \sum_{t \in B} \epsilon_i(t) S_j(t) \tag{B2}$$

$$\Delta K_{ia} = \frac{\eta}{p} \sum_{t \in B} \epsilon_i(t) \mu_{d-1,a}(t) \tag{B3}$$

$$\Delta h_{0i} = \frac{\eta}{p} \sum_{t \in B} \epsilon_i(t) \tag{B4}$$

Here, B denotes the current minibatch and p the minibatch size, η is the learning rate, and $\mu_{d-1,a}(t)$ is the activation of hidden unit a in the final hidden layer $d-1$ at time t .

There is a difference between this problem and a standard SGD computation for a network without recurrence. Here, the forward pass through the layers at time t in some chorale requires (see Eqns. (1-3)) the hidden unit values activations at time $t-1$. However, these are probably not in the current minibatch of randomly chosen steps, so we don’t have access to this information. Furthermore, in order to know these activations, the ones at $t-2$ are required, and so on all the way back to the beginning of the present chorale. This means that in order to do SGD in this problem we must, before each

learning step, run a full forward pass through all time steps and keep track of the $\mu_{l,a}(t)$ at all l and t .

The remaining learning rules, for the J_l and M_l , can be written simply in terms of effective target errors on hidden units, $\delta_{l,a}(t)$.

$$\Delta J_{0,ai} = \frac{\eta}{p} \sum_{t \in B} \delta_{0,a}(t) S_i(t) \quad (\text{B5})$$

$$\Delta J_{l,ab} = \frac{\eta}{p} \sum_{t \in B} \delta_{l,a}(t) \mu_{l-1,b}(t) \quad (\text{B6})$$

$$\delta_{d-1,a}(t) = X_{d-1,a}(t) \left[\sum_i \epsilon_i(t) K_{ia} + \sum_b \delta_{d-1,b}(t+1) M_{d-1,ba} \right] \quad (\text{B8})$$

with

$$X_{d-1,a}(t) = 1 - \mu_{d-1,a}^2(t) \quad (\text{B9})$$

(the derivative of the activation function). The first term describes the backpropagation at time t from output errors at units i , through the K matrix to hidden unit a in the last hidden layer. The second term describes backpropagation in time (BPTT) of effective errors on unit b in the last hidden layer, via the M_{d-1} matrix, to unit a in that same layer one step later. Note

$$\delta_{l,a}(t) = X_{l,a}(t) \left[\sum_b \delta_{l+1,b}(t) J_{l+1,ba} + \sum_b \delta_{l,b}(t+1) M_{l,ba} \right] \quad (\text{B10})$$

In both Eqns. (B8) and (B10), we need to know the effective target on units in the same layer one time step later than t . In a conventional BPTT calculation with only a single layer, one conventionally works back iteratively one step at a time in the same way we worked back in through layers in the above equations. Here, instead, taking advantage of the fact that we have calculated all the $\delta_{l,b}(t)$ in the previous learning step, we can simply shift that array of δ 's by one time step and use that on the right hand side of Eqns. (B8) and (B10). We also found it advantageous to smooth this process by using the average of the δ 's from the previous two steps, rather than just those from the most recent step. In either case, the result is not the exactly the

for $1 \leq l \leq d-1$, and

$$\Delta M_{l,ab} = \frac{\eta}{p} \sum_{t \in B} \delta_{l,a}(t) \mu_{l,b}(t-1) \quad (\text{B7})$$

for $0 \leq l \leq d-1$. The effective target errors can be computed, starting starting from the target output errors, by backpropagation through layers and time steps, as we now describe.

First, the error backpropagation through the net at every time t starts with the first step

that the first term doesn't change t (propagation forward and back in the network is, by construction, instantaneous), and the second term doesn't change the layer index (the M matrices describe intralayer interactions). In the program, these calculations for different t are effectively simultaneous (done in parallel).

Now it is simple to extend this, recursively, to layers with smaller l :

solution of these equations, but if the learning is converging to a stationary solution, it can work. In practice, we find satisfactory convergence for slow enough learning rates.

In both the forward and back-propagation parts of the learning algorithm, it is necessary to prevent information to cross boundaries between successive chorales in the training example sequence. We do this by, at each learning step, setting the hidden unit activations $\mu_{l,a}(t)$ and the effective target errors $\delta_{l,b}(t)$ to zero whenever t is the first chord in a chorale.

As described in the main text, the networks were run using this kind of BPTT and SGD with a minibatch size $p = 300$. The cost function was the negative log likelihood of the data under the

model. Exceptionally, in the case of the learning runs described in Section 4 for two hidden layers, full gradient descent was used. However, SGD was used in the aging calculations for $d = 2$ and the learning in them showed no significant difference from the full gradient descent calculations.

Both the feedforward matrices J_a (except the initial input matrix J_0) and the intralayer recurrent matrices M_a were initialized to be orthogonal. J_0 was initialized as random with elements of variance $0.1/N_v$, with N_v the input dimensionality. The output matrices K and W were initialized to zeros. We haven't found it necessary to include biases in the inputs to any units except the outputs, presumably because we rescaled our inputs to have zero mean and all the connection matrix elements are also zero-mean.

The orthogonality of the M_a was enforced

throughout the learning by the following procedure: After the weight changes were made at each learning step, a singular value decomposition of each matrix was made and all the singular values were set to 1.

Initial learning rates ranged from 10^{-3} for single-layer networks down to 10^{-4} for 10-layer networks. For $d = 5$ and 10, we discovered that if such rates are maintained, the NLL would show chaotic spiky fluctuations well before the target value (usually 0.01) was reached. Therefore, learning was usually done for 2×10^5 iterations at a time, and the learning rate was lowered, typically by a factor of 2, whenever these fluctuations started to occur. Final learning rates were as low as 2.5×10^{-5} for $d = 5$ and 1.25×10^{-5} for $d = 10$ (in both cases for $w \leq 60$). Typical learning runs required 2 to 10 million iterations and took 40-150 hours on MacBook Pros with an M1 or M3 processor.

-
- [1] M. Geiger, S. Spigler, S. d'Ascoli, L. Sagun, M. Baity-Jesi, G. Biroli, and M. Wyart, *Phys. Rev. E* **100**, 012115 (2019).
 - [2] S. Spigler, M. Geiger, S. d'Ascoli, L. Sagun, G. Biroli, and M. Wyart, *J. Phys. A: Mathematical and Theoretical* **52**, 474001 (2019).
 - [3] M. Baity-Jesi, L. Sagun, M. Geiger, S. Spigler, G. B. Arous, C. Cammarota, Y. LeCun, M. Wyart, and G. Biroli, in *International Conference on Machine Learning* (PMLR, 2018) pp. 314–323.
 - [4] L. F. Cugliandolo and P. Le Doussal, *Phys. Rev. E* **53**, 1525 (1996).
 - [5] A. Crisanti, H. Horner, and H. J. Sommers, *Z. Phys. B Condensed Matter* **92**, 257 (1993).
 - [6] J. Hertz, D. Sherrington, and T. M. Nieuwenhuizen, *Phys. Rev. E* **60**, R2460 (1999).
 - [7] N. Boulanger-Lewandowski, Y. Bengio, and P. Vincent, in *Proceedings of the 29th International Conference on Machine Learning*, Edinburgh, Scotland, UK, 2012 (2012).
 - [8] A. M. Saxe, J. L. McClelland, and S. Ganguli, arXiv preprint arXiv:1312.6120 (2013).
 - [9] J. Pennington, S. Schoenholz, and S. Ganguli, *Advances in neural information processing systems* **30** (2017).
 - [10] J. R. de Almeida and D. J. Thouless, *J. Phys. A: Mathematical and General* **11**, 983 (1978).
 - [11] D. Sherrington and S. Kirkpatrick, *Phys. Rev. Lett.* **35**, 1792 (1975).
 - [12] E. Gardner and B. Derrida, *J. Phys. A: Mathematical and general* **21**, 271 (1988).
 - [13] G. Györgyi and P. Reimann, *Phys. Rev. Lett.* **79**, 2746 (1997).
 - [14] L. F. Cugliandolo and J. Kurchan, *Phys. Rev. Lett.* **71**, 173 (1993).
 - [15] H. Sompolinsky and A. Zippelius, *Phys. Rev. B* **25**, 6860 (1982).
 - [16] www-etud.iro.montreal.ca/boulanni/icml2012. This link is apparently no longer active; however, the files are available at github.com/czhuang/JSB-Chorales-dataset.